Chinese Journal of
POLYMER SCIENCE

RESEARCH ARTICLE

https://doi.org/10.1007/s10118-026-3661-2
Chinese J. Polym. Sci. **2026**, *44*, 1898–1911

High-performance Polyimide Cuff Tube with Tunable Mechanics and Long-term Biocompatibility for Microvascular Anastomosis

Hui Su[a], Zhou-Quan Sun[a], Yu-Cheng Qiu[b], Yuan-Yuan Zhang[a], Jing Luo[b], Fei Liu[b], Jun Yang[b], Xian-Yu Zhou[b], Yue Zhang[a*], and Yu-Mei Zhang[a*]

[a] *State Key Laboratory of Advanced Fiber Materials, College of Materials Science and Engineering, Donghua University, Shanghai 201620, China*
[b] *Department of Plastic and Reconstructive Surgery, the Ninth People's Hospital, Shanghai Jiao Tong University School of Medicine, Shanghai 200011, China*

Electronic Supplementary Information

Abstract Microvascular anastomosis is a fundamental technique in microsurgery, and the development of suitable cuff tubes is crucial for improving the surgical efficiency and long-term vascular patency. Polyimide, a high-performance polymer, offers excellent thermal stability, chemical resistance, and biocompatibility, making it a promising candidate for microvascular applications. In this study, we employed a dry-jet wet-spinning method using P84 polyimide to fabricate polyimide (PI) cuff tubes. The effects of bore fluid flowrate, dope flowrate, and take-up speed on the structural morphology and mechanical properties of the tubes were systematically investigated. Heat treatment was applied to optimize the mechanical performance. Heat treatment above the glass transition temperature significantly enhances the solvent resistance and mechanical strength without altering the chemical structure. The PI cuff tubes demonstrated negligible cytotoxicity and hemolysis, no genotoxic or immunogenic effects, and no systemic organ toxicity. *In vivo* implantation showed sustained vascular patency and no local inflammatory response for up to 90 days post-operatively. The fabricated PI cuff tubes possessed high structural integrity, tunable flexibility, ideal mechanical properties, excellent biosafety, and outstanding *in vivo* performance, suggesting their strong potential for future clinical translation in microvascular anastomosis and vascular graft applications.

Keywords Microvascular anastomosis; Polyimide; Dry-jet wet-spinning; Transplantation; Cuff technique

Citation: Su, H.; Sun, Z. Q.; Qiu, Y. C.; Zhang, Y. Y.; Luo, J.; Liu, F.; Yang, J.; Zhou, X. Y.; Zhang, Y.; Zhang, Y. M. High-performance polyimide cuff tube with tunable mechanics and long-term biocompatibility for microvascular anastomosis. *Chinese J. Polym. Sci.* **2026**, *44*, 1898–1911.

INTRODUCTION

Vascular anastomosis is an important part of microsurgery, and the timing and patency of vascular anastomosis have a great impact on the success of surgery.[1,2] The cannula technique is usually used for anastomosis of microvessels with a diameter of less than 2.0 mm, and different microvessels require the appropriate diameter of the cannula for surgery to facilitate intraoperative operation, improve vascular patency, and shorten the duration of the surgery.[3–5] Owing to the delicate operation of microsurgery, mechanical properties of small-diameter cannulae are required. Meanwhile, cannula instability may cause an inflammatory reaction and the formation of foreign body granuloma in and around the inner wall of the vessel after cannula implantation. Therefore, the material stability, mechanical properties, size, and biosafety of the trocars are the keys to enabling them to be widely used in animal experiments and even in clinical practice, and the use of some highly stable polymers is more likely to achieve the desired results.

Polyimide (PI) is flexible, lightweight, heat-resistant, and chemically resistant compared to other resistant materials (polytetrafluoroethylene (PTFE), polypropylene (PP), and polyethylene (PE), *etc.*), which makes it a promising polymer for medical applications.[6–9] Its biocompatibility has been evaluated for use in the fabrication of implantable medical devices, construction of flexible neuroelectrode arrays, and as a coating for neuroprostheses.[10–12] In the field of wearable medicine, PI has been processed into ultra-thin and flexible films to monitor various physiological parameters of the human body in real time, providing data support for personal health management and early warning of diseases.[13,14] In orthopaedic repair, PI has been compounded with bioactive ceramics to create bone repair scaffolds, thereby accelerating the repair process of bone damage.[15,16] Importantly, PI has also shown potential for applications in the field of artificial blood vessels and endovascular catheters. Anastomosis and repair of the retinal veins in living porcine eyes have been performed using PI tubes as artificial blood vessels.[17] In addition, when used as intravascular catheters, solutions containing target agents can be precisely manipulated for injection into arteries that supply target tissues through intravascular

* Corresponding authors, E-mail: zhangyue@dhu.edu.cn (Y.Z.)
E-mail: zhangym@dhu.edu.cn (Y.M.Z.)
Received December 1, 2025; Accepted March 11, 2026; Published online May 27, 2026

catheters.[18,19] Although PI have demonstrated excellent stability and performance in many applications, current studies do not provide an in-depth analysis of the processing and specific implantation properties of micron-sized PI cuff tubes.

PI exhibits extremely high molecular chain rigidity and strong intermolecular forces, resulting in a high glass transition temperature, melting point, and melt viscosity. This makes melt extrusion challenging, and it is difficult to maintain the structural stability and mechanical properties of the material during processing. To investigate the mechanical properties of PI and its potential use in microvascular anastomosis, this study employed a dry-spray wet-spinning process to prepare PI cuff tubes using P84 as the raw material and *N*-methylpyrrolidone as the solvent. By adjusting the spinning conditions such as bore fluid flowrate, dope flowrate, and take-up speed, the microstructure and size of the cuff tubes were modified. Following thermal setting, cuff tubes with varying degrees of stiffness were obtained to investigate the influence of thermal treatment conditions on their morphology and mechanical properties, and to determine the optimal cuff tubes for surgical operability. The vascular sleeve technique was used to anastomose the arteries of the hind limbs of rats, and the blood flow rate and pathological changes at the anastomosis site were observed within one month post-surgery to assess its convenience and safety, with the aim of meeting the needs of clinical physicians.

EXPERIMENTAL

Materials

Polyimide (PI, Grade: P84) was supplied by Zeshancheng New Materials (Wuhan) Co., Ltd., *N*-methylpyrrolidone (NMP), ethanol (EtOH), tetrahydrofuran (THF), and *N*-hexane were of analytical grade, and polydimethylsiloxane (Sylgard 184) of industrial grade, imported from the United States, was purchased from Sinopharm Chemical Reagent Co., Ltd. Deionized water was then prepared. PTFE tubes (inner diameter of 0.6 mm and outer diameter of 0.8 mm) were obtained from Guangdong Dechuang New Materials Co., Ltd.

Preparation of PI Cuff Tubes

Before preparing the P84 solution, first dry the P84 in an oven at 150 °C for 4 h, and then the P84 particles were dissolved in NMP. Swelling was performed at 40 °C for 30 min, followed by stirring and dissolution at 80 °C for 3 h to obtain a P84 solution with a mass fraction of 30 wt%. The solution was then left to stand overnight to remove bubbles. Subsequently, the P84 spinning solution was injected into a metering pump under nitrogen pressure of 0.3 MPa. A peristaltic pump was activated to adjust the bore fluid flow rate. The bore fluid content was fixed at NMP/H_2O volume ratio of 90/10. The spinning solution is slowly extruded through a single-hole spinneret with an outer diameter of 1.0 mm and an inner diameter of 0.4 mm, forming a cuff stream. The stream passes through a 5 cm air gap (at 25 °C and 65% relative humidity) into a coagulation bath (30 wt% NMP aqueous solution at 20 °C), where it solidifies and forms a tube. The tubes were then drawn, washed, rolled, and collected. The newly formed cuff tubes were removed from the rollers and immersed in a deionized water bath, and the water was changed every 6 h to remove residual solvents and non-solvents. After soaking for 2 days, the cuff tube was subjected to solvent exchange using ethanol/hexane. The tube was first immersed in ethanol for 30 min, with fresh ethanol replaced every half hour, which was repeated three times. The same procedure was repeated three times using hexane, after which the tube was hung to dry in a fume hood.

The bore fluid flowrate was varied between 0.5 mL/min and 1.2 mL/min, while the dope flow rate and take-up speed were fixed at 1.12 mL/min and 5.90 m/min, respectively, to investigate the effect of the bore fluid flowrate on the dimensions of the cuff tubes. The dope flowrate was varied between 0.67 mL/min and 1.35 mL/min, while the bore fluid flow rate and take-up speed were fixed at 0.5 mL/min and 5.90 m/min to investigate the effect of dope flowrate on the performance of cuff tubes. The take-up speed was varied within the range of 3.53–9.44 m/min, while the bore fluid flowrate and dope flowrate were fixed at 0.5 and 1.12 mL/min, respectively, to investigate the effect of take-up speed on the performance of cuff tubes.

Heat treatment was performed on the tubes to improve their mechanical properties of PI cuff tubes. The heat treatment temperature was varied between 240 and 440 °C, and the treatment duration was set to 2, 5, or 10 min depending on the temperature.

Characterization

FESEM (Hitachi, Model S-4800, Japan) was used to observe the morphologies of the as-prepared and thermally annealed PI cuff tubes. The samples were fractured in fluid nitrogen and sputtered with gold before the SEM analysis. XRD analysis was performed using an X'pert Pro diffractometer with Cu$K\alpha$ radiation (λ=0.154 nm) to investigate the aggregation structures, with a 2θ scanning range of 10°–60°. FTIR-ATR measurements were conducted using a Nicolet iS 50 spectrometers to analyze chemical functional groups, collecting spectral data in the 400–4000 cm^{-1} wavenumber range.

DSC-TG: the thermal stability and thermal decomposition behavior of the cuff tube were tested using a German NETZSCH STA 449 F5. An appropriate amount of the sample (5–10 mg for conventional samples) was uniformly placed in an alumina crucible. The temperature was increased from room temperature to 800 °C at a heating rate of 10 °C/min under a nitrogen atmosphere (flow rate: 50–100 mL/min), and the heat flow curve (DSC) and weight loss data (TG) were recorded synchronously.

Different PI cuff tubes were tested by room-temperature gel permeation chromatography (Agilent GPC50, column: PLgel 10 μm, MIXED-B). The samples were dissolved in DMAC at a concentration of 1.0 mg/mL. Polymethyl methacrylate (PMMA) with an average molecular weight of 1.0–30.0 kg/mol was used as the standard to obtain the standard curve. A DMAC/0.5% LiCl solution served as the mobile phase (1.0 mL/min), the column temperature was 50 °C, and the injection volume was 100 μL.

Mechanical Properties of PI Cuff Tube

Axial tensile properties test: referring to the test method for the axial tension of artificial blood vessels (ISO 7198:1998), measurements were made using a fiber jig. The test conditions were as follows: a tensile speed of 100 mm/min, clamp spacing of 20 mm, and specimen length of 50 mm. All samples were mea-

sured at a relative temperature and humidity of 25 °C and 50%, respectively. During the stretching process, the cuff tube was not tilted or twisted.

A KES-FB2 pure bending tester was used to evaluate the bending properties of the PI cuff tubes. To reduce the effect of gravity, the test was carried out in a vertical horizontal plane with a clamping distance of 10 mm. During the experiment the moving collet drove one end of the specimen along a fixed trajectory within a certain angle, moving upwards to reach the ultimate curvature, and when the ultimate curvature reached the collet drove the end of the specimen; when the ultimate curvature reached the collet, it drove the end of the specimen, and when the ultimate curvature reached the collet drove the end of the specimen. During the test, the two fixed ends of the PI cuff tubes were clamped with two collets (fixed and mobile) and the specimen was free to bend between the two collets. The bending stiffness of the cuff tubes was calculated for the test curvatures of 0.3, 0.7, and 1.

A KES-FB3 tester was used to test the PI Hollow tubes for 120 cN Radial compression property tests, and the compression elasticity indices of the PI tube were obtained by measuring the change in specimen thickness under both light and heavy loads and after removal of the load.

In vitro Cytotoxicity Evaluation

Preparation of the PI material extracts

The PI particles were ultrasonically cleaned with ultrapure water for 15 min, dried naturally, and sterilized in an autoclave at 120 °C for 30 min. RPMI-1640 culture medium (G4535, Servicebio, Wuhan, China) was used as the extraction medium for the cellular experiments, whereas 0.9% NaCl solution was used for the other experiments. PI was dissolved in the solvent at a proportion of 0.2 g/mL and placed in a cell culture incubator at 37 °C, 5% CO_2 for 72 h to obtain PI extracts. According to the mass-to-extracting medium ratio of 0.4, 0.2, and 0.1 g/mL, the extracts were prepared at concentrations of 2, 1, and 0.5 times the standard concentration, respectively. They were then filtered through a 0.22 μm bacterial filter (BD Falcon, USA) and stored at 4 °C for later use.

Scratch assay

L929 cells were inoculated in six-well plates (Corning, USA) at a density of 3×10^5 cells/well and cultured until the cell density exceeded 90%. Scratches were made on a vertical plate using a 200 μL pipette (Corning, USA), and the detached cells were washed with phosphate-buffered saline (PBS). The culture medium was replaced with a normal culture medium (negative control group) or PI extract (experimental group), and the culture was continued for 24 h. Scratched areas of the two groups were photographed at 0 and 24 h under an inverted microscope (Olympus IX73, Japan). The scratched area was statistically analyzed using ImageJ software.

Genotoxicity test

The genotoxicity and oncogenicity of the PI cuff tubes were evaluated using the Ames Test Kit (0211021, IPHASE, Bioscience Co., LTD., China) and the *in vitro* Mammalian Chromosomal Aberration Test Kit (0221015, IPHASE Bioscience Co., LTD., China). The experimental group was treated with various concentrations of PI extracts, the negative control group received sterile water treatment, and the positive control group was included in accordance with the manufacturer's protocol for sample addition. The samples were prepared based on the stoichiometries presented in Table S1 (in the electronic supplementary information, ESI).

In the Ames test, TA98 and TA100 strains (0211021, IPHASE Bioscience Co., LTD., China) were proportionally added to the culture medium to form the growth mixture. Each group was mixed and distributed into 96-well plates (48 wells per group, 190 μL/well) and placed in an incubator at 37 °C for 24 h. Twenty microliters of a growth indicator were added to each well, and the reverted colonies in each group were recorded after 48 h of incubation.

For the mammalian chromosome aberration assay, CHL cells (Cell Bank of the Chinese Academy of Science, Shanghai, China) were selected and adjusted to a density of 1×10^6 cells/mL. The cells were spiked and cultured according to the spiking method described in Table S2 (in ESI). In each group, 0.05 mL of 50 μg/mL colchicine (ST1173, Beyotime, China) was added to 5 mL of the culture solution and incubated for 3 h. Then, cells were collected and counted, and cell suspensions received hypotonic treatment with 0.075 mol/L KCl solution (DB1001, Fuzhou wabcan Biotechnology Co., LTD.). The suspensions were fixed, titrated, stained, and sealed with neutral gum. Chromosomal aberrations were observed and photographed using an Olympus Microscope (Model BX40).

Hemocompatibility test

The hemocompatibility of the PI material was assessed using coagulation, hemolysis, platelet adhesion, and platelet activation assays. In the coagulation test, 50, 100, and 200 mg of cannula particles were added to the normal mixed plasma. The thrombin coagulation time (TT), international normalized ratio (INR), prothrombin time (PT), and partial thromboplastin time (APTT) were determined.

In the hemolysis test, 5 mL of saline, distilled water, and standard extract were placed in a centrifuge tube (Corning, USA), with three parallel controls for each group, and preheated for 30 min at 37 °C. The normal saline group was used as the negative control ((−) control), the distilled water group was used as the positive control ((+) control), and the standard extract group was used as the experimental group. Diluted rabbit erythrocytes (0.2 mL) were added to the samples and shaken. Subsequently, the samples were placed in a water bath at 37 °C for 50 min and centrifuged to obtain the supernatant. The absorbance at 545 nm was measured, and hemolysis rates were calculated using 6 replicate wells for each group. The hemolysis rate was calculated using the following formula:

$$\text{Hemolysis rate} = \frac{(OD_{\text{value of sample}} - OD_{\text{value of negative control}})}{(OD_{\text{value of positive control}} - OD_{\text{value of negative control}})} \times 100 \quad (1)$$

The OD values of absorbance of each group were measured at 545 nm with a microplate reader.

Fresh rat blood was collected in a vacuum tube containing sodium citrate and centrifuged at 1500 r/min for 15 min to obtain platelet-rich plasma. Plasma was incubated with PI or PTFE samples at 37 °C for 2 h. The samples were washed 3 times with normal saline, and the adhered platelets were fixed with 2.5% glutaraldehyde, dehydrated with gradient ethanol, and observed by SEM. In the platelet activation as-

say, P-selectin (CD62p) expression in platelets treated with PI or PTFE was evaluated by flow cytometry to determine the level of activated platelets (CytoFLEX, Beckman Coulter, USA).

Cytotoxicity assay

A CCK-8 kit (CK04, Doijndo, Japan) was used to evaluate the cytotoxicity of the PI. L929 cells (CL-0137, Wuhan Pricella Biotechnology Co., Ltd.) were inoculated into 96-well plates (5×10^3/well) (Corning, USA) for 24 h, and then culture medium was replaced with normal RPMI-1640 medium (negative control group), 1% phenol (Thermo Fisher, USA) (positive control group), or different concentrations of extracts (experimental groups), respectively. After 1, 2, 3, and 4 days of culture, the CCK-8 assay was performed. The absorbance OD values of each group were measured with a microplate reader (Biotek, Synergy H1, USA) at 450 nm after 2 h of treatment, and the relative growth rate (RGR) was calculated using the following formula:

$$RGR = \frac{OD_{value\ of\ sample}}{OD_{value\ of\ negative\ control}} \times 100 \quad (2)$$

Vascular smooth muscle cells (CD5004, Shanghai QiDa Biotechnology Co., Ltd.) were seeded into 96-well plates (5×10^3 cells/well) and the CCK-8 assay was conducted after 1, 3 and 5 days of co-culture as described previously. On Day 2, the cells were stained with a live/dead cell staining kit (C0021, Applygen Technologies Inc., China) and cell viability was evaluated under a fluorescence microscope (Olympus CKX53, Japan).

Antibacterial test

The antibacterial properties of the PI material were evaluated using the colony-counting method. Gram-negative Escherichia coli and Gram-positive Staphylococcus aureus were used as bacterial models. Each group was analyzed three times after 24 h of co-culture. The antibacterial rate was calculated using the following equation:

$$\text{Antibacterial rate}\,(\%) = \frac{\text{cell count of control group} - \text{cell count of PI group}}{\text{cell count of control group}} \times 100 \quad (3)$$

Preclinical Assessment

Rat orthotopic hindlimb transplantation

Male 10- to 12-week-old Lewis rats and male 6- to 8-week-old BALB/c mice were purchased from Sino–British SIPPR/ BK Lab Animal Co., Ltd. (Shanghai, China). All animals were housed in a pathogen-free facility at a standard temperature (24± 2 °C) with a 12 h light/dark cycle. All protocols were approved by the Ninth People's Hospital, affiliated with the Shanghai Jiao Tong University School of Medicine Animal Care and Use Committee) (approval No. SH9H-2021-A983-SB). To assess the biostability of the PI cuff tube, ultrasonic Doppler was employed to detect the *in vivo* degradation of the implants. The cuff tubes were implanted subcutaneously in mice, and their length and diameter were monitored at postoperative days (POD) 7, 14, 30, and 90 to illustrate the degradation of cuff tubes. All the mice were exposed to isoflurane. With the assistance of PI cuff tubes, rat orthotopic hind limb transplantation was performed from one Lewis donor to another Lewis recipient, as described elsewhere (n=6).[20] In the control group, microvascular anastomosis was performed using the hand-sewn technique (n=6). The recipients received a subcutaneous injection of meloxicam (2 mg/kg) before and after the surgery to provide analgesia and prevent inflammation. The recipients were regularly monitored for at least 4 h before returning to the housing facility.

Histopathology and immunofluorescence analysis of peri-tube tissues

Peri-tube muscle tissues from the homografts and hind limbs of naïve rats were obtained at PODs 30 and 90. All specimens were fixed in 4% paraformaldehyde for 24 h. Tissue sections were stained with hematoxylin and eosin after paraffin embedding, and the local inflammatory response was observed.

For immunofluorescence staining, complement C3 deposition in peri-tube tissues was detected at PODs 30 and 90 using an anti-C3c rabbit pAb (GB114734-100, Servicebio, Wuhan, China) primary antibody. Anti-rabbit immunoglobulin G (IgG) (GB111738, Servicebio, Wuhan, China) and anti-rabbit immunoglobulin M (IgM) (GB112040, Servicebio, Wuhan, China) were used to detect the deposition of IgG and IgM, respectively. The nuclei were counterstained with 4′,6-diamidino-2-phenylindole (DAPI). Finally, the sections were sealed and photographed using a fluorescence microscope (Leica DMI4000B, Germany). DAPI-stained nuclei are blue, and the positive structures are represented as green light labeled with fluorescein. All images were captured using CaseViewer 2.4 (3DHISTECH. Ltd., Hungary), and the mean fluorescence densities were measured using the ImageJ software.

Detection of cytokine levels in plasma and peri-tube tissues

On PODs 30 and 90, Lewis recipients and naïve rats were subjected to withdrawal of plasma and peri-tube muscle tissue samples, which were then maintained at –80 °C until further use. The levels of interleukin (IL)-2, IL-10, tumor necrosis factor (TNF)-α, and interferon (IFN)-γ were measured using an enzyme-linked immunosorbent assay kit (ELISA kit; R2000, R1000, RTA00, and RIF00, R&D Systems, Minneapolis, MN, USA) in compliance with the manufacturer's instructions.

Evaluation of renal and hepatic function

The levels of indicators of hepatological function such as aspartate aminotransferase (AST) and alanine aminotransferase (ALT), renal function (creatinine and urea), aspartate aminotransferase (AST), and alanine aminotransferase (ALT), were determined and compared between recipients and naïve rats at PODs 30 and 90. The liver and kidney tissues of PI and control groups were biopsied on POD 90, fixed in 4% paraformaldehyde for 24 h, then embedded in paraffin, sectioned, and stained hematoxylin and eosin (H&E) staining to evaluate pathological inflammations and organ lesions.

Statistical Analysis

Data are expressed as the mean ± SD (at least three or more independent samples) and compared between groups using the unpaired Student's t-test. The normality of each dataset was assessed using the Shapiro–Wilk test. All statistical tests were performed using GraphPad Prism 8.0 software (La Jolla, California, USA). $^{*}p < 0.05$, $^{**}p < 0.01$, $^{***}p < 0.001$, $^{****}p < 0.0001$, ns: not significant.

RESULTS AND DISCUSSION

Cuff Technique for Microvascular Anastomosis

Microvascular anastomosis is an indispensable foundational technique in tissue transplantation, trauma repair, organ re-

plantation, and the treatment of vascular diseases and is, particularly important in the field of microsurgery. Its primary objective is to rapidly and stably restore blood flow, ensuring adequate blood supply to the graft or distal tissue. However, microvascular diameters typically measure less than 1 mm, resulting in extremely limited surgical space, which imposes stringent demands on the surgeon's microsurgical suturing skills. Fig. 1(a) illustrates the surgical procedure used for microvascular anastomosis. The surgical site was located in the thigh, with the femoral artery and femoral vein exposed for manipulation. The anastomosis process involves the following steps: first, the vessel is cut, and one end is inserted into a microtube with a flange. The vessel wall was everted using a flanging operation to cover the opening of the microtube. Subsequently, the other end of the vessel was aligned and inserted into the microtube and fixation was achieved through suture ligation, thereby establishing an end-to-end connection between the vessel ends.

The anastomosis tube was made of PI material to achieve an efficient and reliable anastomosis process. PI has excellent mechanical strength, flexibility, and thermal stability, as well as good dimensional machinability and biocompatibility, enabling it to meet the dual requirements of wall support and tissue safety in microvascular anastomosis. Additionally, its low surface energy properties help inhibit the adhesion of proteins and cells in the blood, reduce the risk of thrombosis and improve post-anastomosis vascular patency. Fig. 1(b) shows an *in vivo* image of a rat femoral artery anastomosis

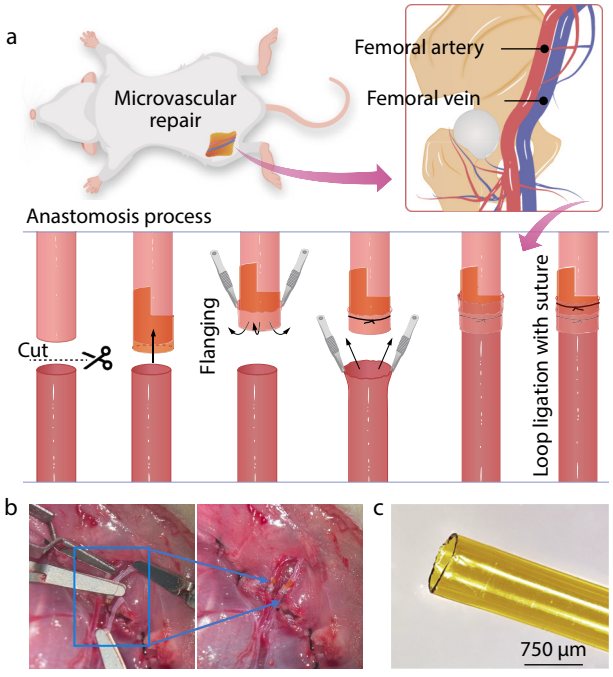

Fig. 1 Cuff technique for microvascular anastomosis. (a) Surgical diagram of microvascular repair of the femoral artery/femoral vein in rats. Basic principles of the cuff technique involve pulling the vessel through a polyamide cylinder and everting the vessel, thereby exposing the endothelial surface. For anastomosis, the vessel and cuff can then be inserted into the donor vessel and secured with a tie. (b) Intraoperative images of femoral artery anastomosis surgery in rats. (c) Microscopic photograph of PI cuff tube.

surgery. The magnified area shows the detailed procedure at the anastomosis site, demonstrating the feasibility of using PI microtubes for vascular connections. In addition, Fig. 1(c) presents a microscopic image of the microvascular anastomosis tube made from PI material, with an outer diameter of approximately 600 μm, designed to facilitate mechanical-assisted microvascular anastomosis.

Effect of Spinning Process on Microstructure and Properties of the PI Cuff Tube

To meet the requirements for microvascular anastomosis, it is necessary to comprehensively investigate the effects of bore fluid flow rate, dope flowrate, and take-up speed on the size structure and mechanical properties of the PI cuff tube during the dry-jet-wet-spinning process (Fig. 2a). The morphology of the PI cuff tube spun at different bore fluid flow rates is shown in Fig. 2(b) and Fig. S1(a) (in ESI). As the bore fluid flowrate increased, the flowrate ratio of the dope to the bore fluid decreased, and both the inner and outer diameters of the cuff tube increased, with the inner diameter showing a more pronounced increase, while the thickness gradually decreased. When the bore fluid flowrate was 1.2 mL/min, the inner and outer diameters of the cuff tube were (564.20±1.27) and (686.65±7.54) μm, respectively. When the flowrate exceeded 1.2 mL/min, the tube wall became too thin, resulting in poor self-supporting performance and preventing proper formation. This is because the bore fluid, as the internal filling fluid, increases the pressure on the inner wall of the tube when its flow rate increases, preventing the tube from maintaining its shape. Moreover, changes in the bore fluid flow rate affect the mass transfer process between the cuff's interior and exterior, thereby influencing the cuff's coagulation rate and structural formation. Higher bore fluid flow rates accelerated the coagulation rate within the tube, while the external coagulation rate remained relatively slower, leading to a thinner wall thickness (Fig. 2c). Additionally, as the bore fluid flow rate increased, the mechanical properties of the PI cuff tube decreased (Fig. 2d). This is primarily because the higher bore fluid flow rates accelerate the solvent diffusion within the tube. During coagulation, the molecular chains cannot fully orient and align, resulting in a loose internal structure with numerous defects and voids. This reduced the ability of the tube to resist tensile forces, thereby decreasing the tensile strength.

The dope flow rate has a significant impact on the dimensional structure of the PI cuff tubes, particularly in terms of diameter uniformity and cross-sectional shape. Under constant spinning conditions, maintaining an air gap of 5 cm, bore fluid flowrate of 0.5 mL/min, and bore fluid concentration of NMP/H_2O at 90/10, the effects of different dope flow rates on the PI cuff tube were investigated. The cross-sectional morphologies of the PI cuff tubes at different doping flow rates are shown in Fig. 2(e) and Fig. S1(b) (in ESI). As the dope flow rate increased, the structure of the cuff tube became more compact, with a slight increase in the outer diameter and wall thickness, whereas the inner diameter remained largely unchanged (Fig. 2f). As shown in Fig. 2(g), the mechanical properties and elongation of the tubes decreased when the doping flowrate exceeded 0.9 mL/min. The strength decreased significantly when the dope flowrate was over 1.12 mL/min. This may be the reason why the relatively low shear stress on

https://doi.org/10.1007/s10118-026-3661-2

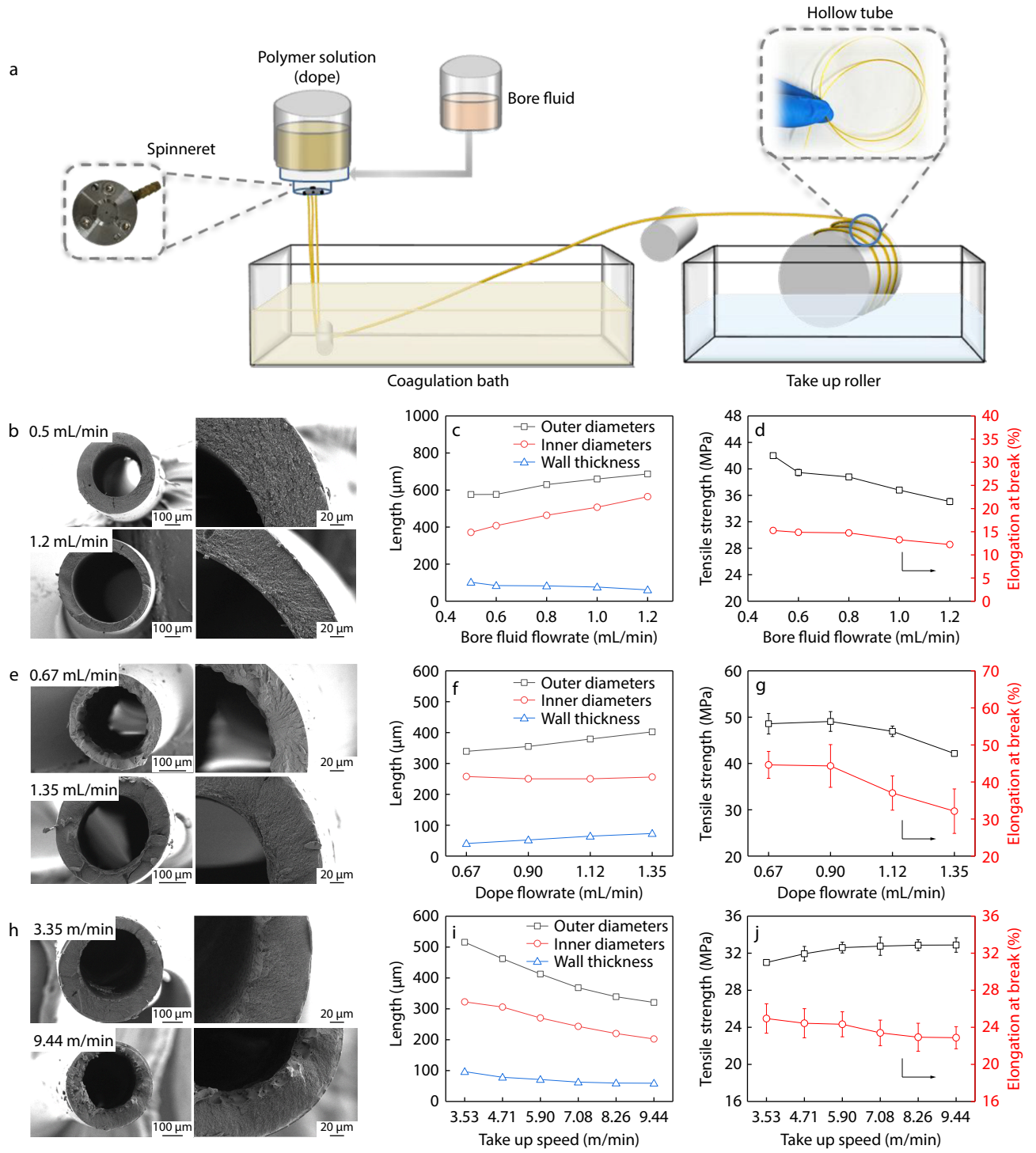

Fig. 2 Effect of spinning process on microstructure and properties of the PI cuff tube. (a) Flow chart of the wet spinning process for preparing PI cuff tube. The effects of (b–d) bore fluid flowrate; (e–g) dope flowrate; (h–j) take-up speed on structural morphology, tube size and mechanical properties of PI cuff tube.

the spinning solution at the exit of the spinneret was relatively low, allowing the spinning solution to distribute more uniformly around the spinneret. Upon entering the coagulation bath, the coagulation process became more stable, which was conducive to the formation of uniform diameters and regular cross-sectional shapes. Conversely, when the dope flow rate increased, the shear stress on the dope at the spinneret exit increased, and the dope flowrate became more complex, leading to fluctuations and unevenness. This unevenness is transmitted to the coagulation bath, causing different coagulation rates in different parts of the tube, thereby affecting the uniformity of the diameter and cross-section-

al shape. In addition, at higher dope flow rates, the contact time between the dope and coagulation bath was reduced, resulting in insufficient mass transfer and heat transfer processes. Upon further increasing the bore fluid/dope flow rate ratio to 3.6, the wall thickness no longer decreased significantly. However, excessively thin walls would reduce the self-supporting capability of the tube, making it prone to collapse. Therefore, a dope flowrate of 1.12 mL/min was selected to ensure that the outer diameter of the tube remained below 500 μm while maintaining a good self-supporting performance.

Take-up speed is another important parameter that influences the structure of the PI cuff tube during the spinning process. As the take-up speed increases, the structure of the cuff tube becomes more compact. Increasing the take-up speed also resulted in a decrease in the wall thickness, inner diameter, and outer diameter of the PI cuff tube (Figs. 2h and 2i, Fig. S1c in ESI), while the strength of the tube increased and the elongation at break decreased (Fig. 2j). Increasing the take-up speed causes the PI polymer chains to become more tightly packed, reducing the free volume between polymer chains. This could partially resist water ingress and lower the double-diffusion rate, thereby reducing the formation of tubular pores and resulting in smaller tube diameters. These results indicate that precise control of the spinning parameters could optimize the dimensions and structure of the cuff tube to suit microvascular applications, establishing a solid foundation for the application of PI cuff tubes in vascular anastomosis.

Effect of Heat Treatment on the Performance of PI Cuff Tube

To select a cuff tube with better surgical operability, it must be sufficiently flexible to facilitate manipulation during surgery, while also being sufficiently robust to withstand the mechanical forces encountered within the body. By subjecting the cuff tube to relaxation heat treatment, the molecular chains within the PI could rearrange and adjust, forming a more stable structure. As shown in the TG-DSC curve of the P84 raw material (Fig. S2 in ESI) and the glass transition temperature (T_g) was 320 °C. Thermal treatment was performed at temperatures below, equal to, and above the T_g. As the heat treatment temperature increased, the color of the cuff tubes gradually darkened (Fig. 3a). The solubility test of the cuff tube could reflect its structure to some extent. As shown in Fig. 3(a), when the original and heat-treated cuff tubes were immersed in NMP solvent at a concentration of 0.5% for 30 min, the original and those heat-treated at 240 and 320 °C completely dissolved, whereas those heat-treated at 400 °C showed no significant changes and did not dissolve even after 12 h, demonstrating excellent solvent resistance. This indicates that the chemical structure of the polymer undergoes changes at high temperatures. As the temperature and duration of heat treatment gradually increased, the structure of the PI cuff tubes became more compact (Fig. S3 in ESI), with reduced inner and outer diameters and thinner walls. The inner and outer diameters remained almost unchanged at 380 °C (Table S3 in ESI). When the temperature of heat treatment was below the T_g, the tensile strength and elongation at break decreased significantly, reaching 8.02 MPa and 11.17%, respectively (Table S4 in ESI). Compared with untreated samples, these values decreased by 22.8% and 28.2%, respectively. This may be due to water adsorption and hydrolysis of the PI cuff tube during processing below T_g, resulting in a decrease in the molecular weight (M_w) (Fig. 3b). When the temperature was further increased above T_g, the mechanical properties of the PI cuff tube gradually improved, which may be attributed to an increase in M_w, as higher temperatures induced further cross-linking or rearrangement of the polymer chains. At temperatures above 400 °C, the mechanical properties slightly decreased (Table S4 in ESI). This may be due to the excessive temperature causing thermal degradation or carbonization of PI, leading to a decrease in mechanical strength.

To better understand these changes, FTIR spectroscopy and XRD patterns were used to elucidate potential chemical transformations and microstructural evolution. Fig. 3(c) shows the FTIR spectra of the PI cuff tubes after 10 min of heat treatment at different temperatures. The FTIR spectra of the tubes remained largely consistent before and after heat treatment. The peaks at 721, 1099, 1366, 1727, and 1780 cm^{-1} corresponded to the C=O bending vibration of the imide ring, the C−N−C stretching vibration, the C−N stretching vibration, and the C=O symmetric and asymmetric stretching vibrations, respectively, indicating that heat treatment did not affect the main chain structure of the tubes.[21] In the XRD patterns (Fig. 3d), all PI cuff tube samples exhibit broad peaks, characteristic of an amorphous structure. The Bragg peak intensity increased as the heat treatment temperature increased. According to Bragg's law: $\lambda = 2d\sin\theta$ (where d is the average interchain distance of the polymer segments, λ is the X-ray diffraction wavelength, and θ is the Bragg angle).[21, 22] The average interchain distance gradually decreases. This indicates that during the heat treatment, the PI polymer chains undergo movement, resulting in a more compact chain structure. Fig. 3(e) shows the weight loss of the untreated and heat-treated PI cuff tubes at different temperatures. For PI cuff tubes with heat treatment temperatures below 240 °C, the weight loss rate of the samples was approximately 2.41%. For PI cuff tubes with heat treatment temperatures above 240 °C, the weight loss rate of the samples decreased to below 0.96%, which was primarily due to the significant removal of adsorbed moisture during the heat treatment process.[23] Overall, the heat treatment enhanced the mechanical properties, and PI cuff tubes with different hardness levels could be obtained by controlling the temperature and duration of the heat treatment (Table S5 in ESI).

The primary performance characteristics of microvascular anastomosis tubes are the ability to maintain a certain level of strength or hardness, durable resistance to mechanical fatigue, and ability to withstand the impact of strong blood flow over an extended period without rupturing or deforming. Based on the experimental results obtained under the aforementioned spinning conditions, we selected a bore fluid flowrate of 1.2 mL/min, a dope flowrate of 1.12 mL/min, and a take-up speed of 3.53 m/min as the spinning parameters. The material was then subjected to a 10-min heat treatment at 380 °C to produce a PI cuff tube with optimal comprehensive performance. The bending and compression properties were tested (Fig. 3f and Fig. S4 in ESI) and compared with those of commercial medical sleeves (polypropylene, PP; polytetrafluoroethylene, PTFE) and elastic tubes (silica gel). The PI cuff tube demonstrated a bending resistance comparable to that of commercial sleeves under a high curva-

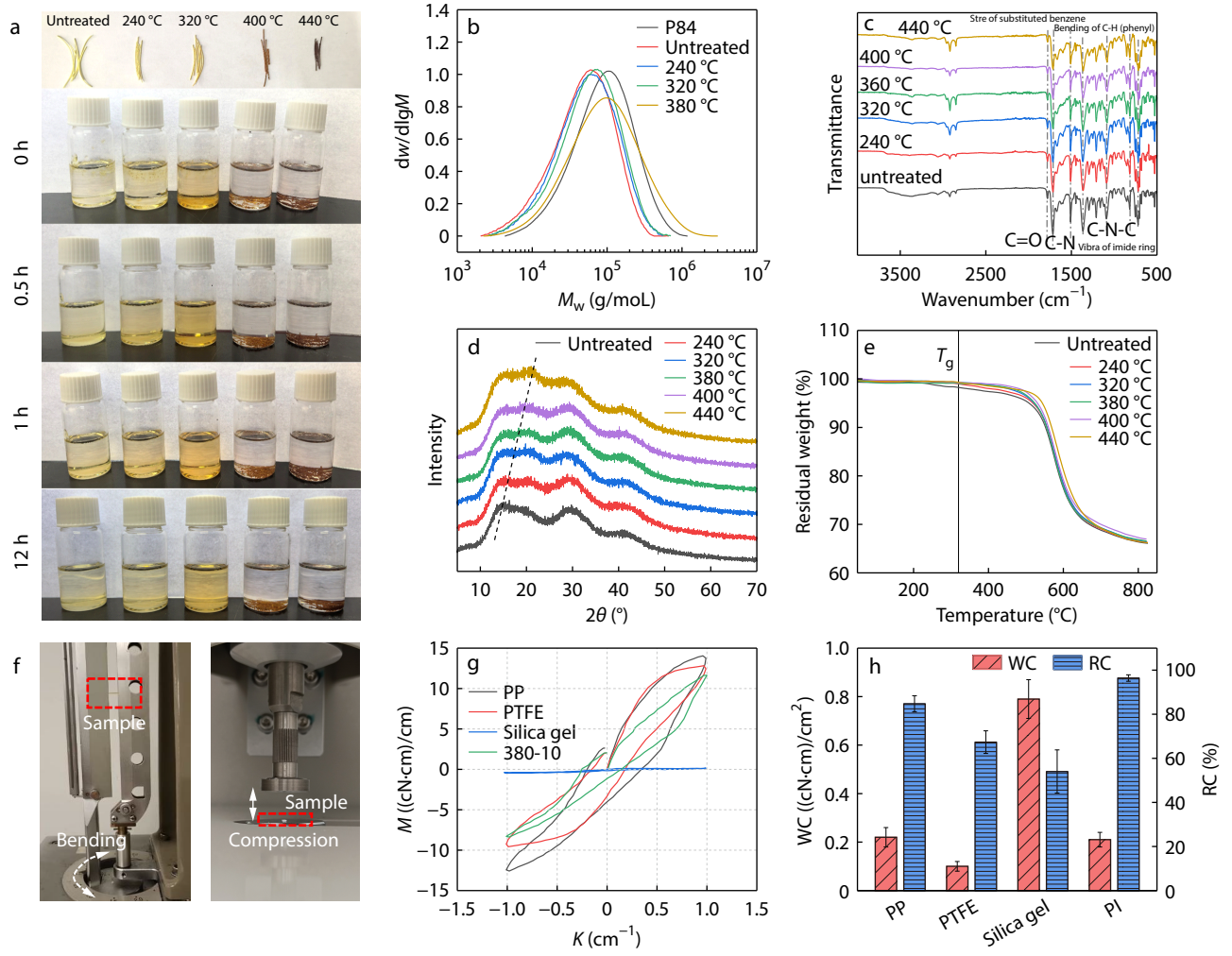

Fig. 3 Effect of heat treatment on the performance of PI cuff tube. (a) Colour changes and dissolution properties of PI cuff tubes at different heat treatment temperatures; (b) Molecular weight (M_w), (c) FTIR spectra, (d) XRD patterns and (e) TG curves of PI cuff tubes at different heat treatment temperatures; (f) Photos of bending and compression tests; (g) Comparison of bending and (h) compression properties of medical-grade PP, PTFE sleeves, silica gel tube, and PI cuff tube. WC represents compression specific work, RC represents compression recovery rate.

ture (Fig. 3g and Table S6 in ESI). Furthermore, the PI cuff tube exhibited superior compression resistance compared to PP and maintained an optimal compression recovery performance (Fig. 3h and Table S7 in ESI). In short, the prepared PI cuff tube possessed excellent structural stability and surgical operability, fully meeting the mechanical requirements for supporting the microvasculature.

Biosafety Assessment of the PI Cuff Tube

The *in vitro* biosafety of the PI was evaluated. In the hemocompatibility evaluation, the plasma coagulation function indicators were within the normal range after treatment with different concentrations of PI particles (Fig. 4a). Hemolysis test revealed that the PI material did not induce obvious hemolysis of erythrocytes, even at high concentrations. The hemolysis rate of the PI material was 0.96%, which is less than 5% and meets the requirement of the hemolysis rate of biomedical materials (Table S8 in ESI). The adhesion of platelets on cuff tubes was qualitatively characterized using SEM images. After co-incubation of the PI or PTFE samples with platelet-rich plasma for 2 h, a large cluster of platelets adhered to the PTFE surface (Fig. S5a in ESI). However, the number of platelets adhered to the PI surface decreased significantly compared to that of PTFE. In the platelet activation assay, the level of activated platelets in the PI group was significantly lower than that in the PTFE group (positive control), illustrating the anti-thrombogenic properties and hemocompatibility of the PI material. (Figs. S5b and S5c in ESI). The reduction in platelet adhesion and activation further contributes to the long-term patency of the anastomosed vessels. For the CCK-8 assay, cells were cultured with varying concentrations of PI extract, and the optical density (OD) values in the experimental groups at various time intervals showed significant differences, compared to those in the positive control group (p <0.05) (Fig. 4b). As the concentration increased, there was no significant difference compared with the negative control group (p>0.05). Considering that the relative cell growth rates were maintained over 95% in the experimental groups, the cytotoxicity of the PI material was evaluated as grade 0–1, illustrating the ideal biocompatibility of PI material (Fig. 4c). The live/dead assay of VSMCs also demonstrated that cells proliferated well after treatment with PI extract compared to the control group (Figs. S6a and S6b in ESI). A similar result was found in

https://doi.org/10.1007/s10118-026-3661-2

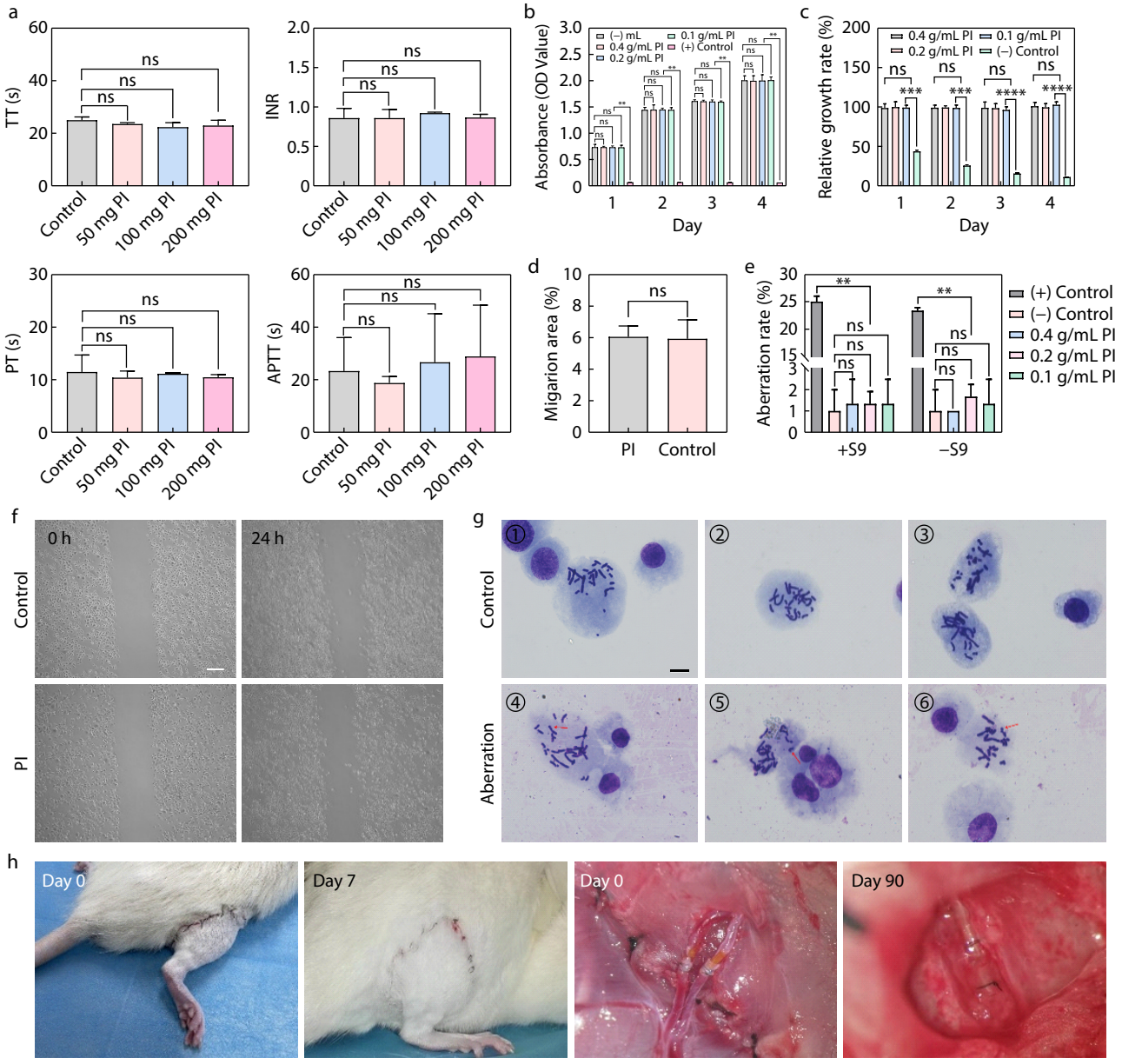

Fig. 4 Biosafety assessment of the PI cuff tube. (a) Coagulation function of TT, INR, PT and APTT of plasma receiving different concentrations of PI particles treatments. (b) Proliferation of L929 cells upon various concentrations of PI extract treatments. (c) Relative growth rates of L929 cells in positive control group and experimental groups of different concentrations. (d) Migration area of L929 cells receiving normal RPMI-1640 medium and PI extract treatments. (e) Aberration rates of CHL cells after 3 h incubation with different concentrations of PI materials in the culture medium. (f) Images of L929 cells migration after treatment with normal RPMI-1640 medium and PI material extract. Scale bar, 200 μm. (g) Chromosome aberrations after the action of the extract on CHL cells. Scale bar, 10 μm. ①–③ show normal chromosomes, with typical chromosome number, morphology and structure. ④–⑥ show aberrated chromosomes: ④ the arrow presents double-stranded aberrations in chromosomes after the action of PI material extract; ⑤ arrow presents ring chromosome after the action of the positive control group; ⑥ arrow presents chromosome defects after the action of the positive control group. (h) Macroscopic images of hindlimb homografts and microscopic images of the PI cuff tubes. Data were presented as the mean ± SD (n=3 independent samples), *p < 0.05, **p < 0.01, ***p < 0.001, ****p < 0.0001, ns: not significant. CHL cells, Chinese Hamster Lung cells; TT, thrombin coagulation time; INR, international normalized ratio; PT, prothrombin time; APTT, partial thromboplastin time.

the CCK-8 assay, which showed no obvious cytotoxicity in the PI group after 1, 3, and 5 days of culture (Fig. S6c in ESI). The good cytocompatibility of the PI material with VSMCs may also enhance vessel patency.

As shown in Figs. 4(d) and 4(f), scratch test results showed no significant difference ($^{*}p$>0.05) in the percentage of L929 cell migration in the scratch area between the experimental and control groups. This confirmed that PI did not affect cell migration, which is critical for angiogenesis in the biological processes of blood vessel healing and vascular network formation. The Ames and *in vitro* mammalian chromosome aberration assays were conducted to assess the genotoxicity of PI

the material. As shown in Table S9 (in ESI), the number of revertant colonies of the TA98 and TA100 strains, with and without the metabolic activation system, was less than twice that of the negative control group, demonstrating a negative Ames test for the PI material. The chromosome aberration rate of CHL cells after PI extract treatment was similar to that of the negative control group ($^{*}p>0.05$) (Figs. 4e and 4g). These results indicated that the PI material possessed no genotoxicity or oncogenicity, providing an important basis for its application in microsurgery. As for the antibacterial test, no significant difference in the inhibition rates for *Escherichia coli* and *Staphylococcus aureus* was observed between the PI and control groups, suggesting that the PI cuff tube was not pro-bacterial and would not induce post-implant infections (Fig. S7 in ESI).

Regarding the *in vivo* stability of the PI cuff tube, ultrasound evaluations on Days 7, 14, 30, and 90 after surgery suggested that the echo intensity of cuff tubes was stable, and no obvious changes in the length and diameter were found throughout the follow-up period (Fig. S8 in ESI). These results indicated that the PI cuff tube could maintain a stable structure *in vivo*.

Rat orthotopic hindlimb homotransplantation was performed using the cuff technique to investigate the efficacy of PI cuff tubes in facilitating vascular anastomosis during microsurgery. The cuff tubes were implanted between the donor and recipient femoral vessels, and no occlusion of the terminal blood flow in the transplanted hind limb was observed seven days after surgery. It was found that all the microvessels (100%) anastomosed with the PI cuff tubes remained patent with intravascular flow upon open exploration at POD 90, indicating a long-term survival of the homografts (Fig. S9 in ESI). In contrast, the 90-day occlusion rate in the hand-sewn group was 33.3% (4/6). The higher vascular patency rate in the PI group suggests that the PI cuff tube can effectively prevent occlusion at the anastomosis site. In addition, no signs of degradation were observed at any time during gross observation, further demonstrating the good stability of the tube structure (Fig. 4h). With a complete vascular healing time of 90 days, the PI cuff tube could serve as a long-term implantable device, that provides continuous mechanical support for the anastomosed vessel and ensure long-term patency.[24]

Evaluation of Cuff-related *In vivo* Immunity and Inflammation

To investigate whether the application of the PI cuff tube induced inflammation *in vivo*, muscle samples around the cuff tube were collected on postoperative days (PODs) 30 and 90 for histological analysis by hematoxylin and eosin (H&E) staining. Diffuse mononuclear cell infiltration was not observed, and there was no notable difference between the PI and naïve rats at any time point (Fig. 5a). The H&E staining results suggested that the PI cuff tube did not evoke an inflammatory response and possessed good biosafety.

Peri-tube muscle tissues were collected at PODs 30 and 90 to investigate the potential immune response induced by implantation of the PI cuff tube. The deposition of immunoglobulin G (IgG), IgM and complement C3c was analyzed by immunofluorescence (Fig. 5b). The mean fluorescence densities of IgG, IgM, and complement C3c in PI recipients and naïve rats were quantified using the ImageJ software. The analysis revealed no notable differences in mean IgG or IgM densities between the PI and control groups at each time point. Furthermore, the deposition of complement C3c was not significant in either group (Fig. 5c). Therefore, these results indicate that the PI cuff tube did not upregulate the level of antibody expression, and no immune response was evoked after device implantation.

Pro- and anti-inflammatory cytokines play critical roles in maintaining local and systemic homeostasis following injury and immune activation. To investigate whether the PI cuff tubes could induce inflammation *in vivo*, the levels of the pro-inflammatory cytokines IL-2, TNF-α, and IFN-γ, and the anti-inflammatory cytokine IL-10 in peri-tube muscle tissues and plasma samples were quantified at PODs 30 and 90. The results of the PI and control groups demonstrated no significant differences in the cytokine levels of IL-2, IL-10, TNF-α, and IFN-γ in tissue samples (Fig. 5d). In addition, the plasma concentrations of these cytokines in PI recipients were comparable to those in naïve rats (Fig. 5e). These findings suggest that no local or systemic inflammatory responses were induced by the implantation of the PI cuff tube, which further confirmed its biosafety in microvascular anastomosis.

The histological responses of liver and kidney tissues were investigated to assess the systemic influence of the PI cuff tube. Liver and kidney tissues were harvested on POD 90 for histological examination. The results showed no signs of pathological inflammation or systemic immune response, such as abnormal mononuclear cell infiltration (Fig. S10a in ESI). Moreover, the plasma levels of aspartate aminotransferase and alanine aminotransferase as indicators of liver damage, and creatinine and urea as indicators of kidney damage were determined in the PI and control groups. In general, all results were within the normal range after the implanta-

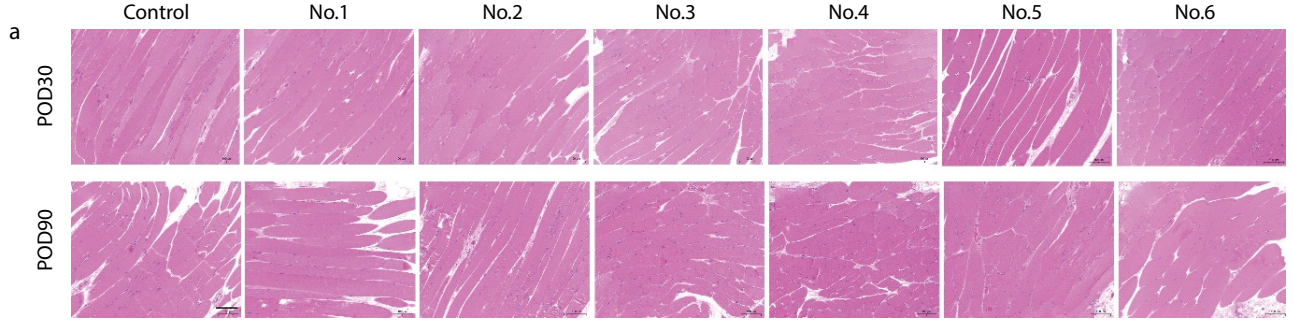

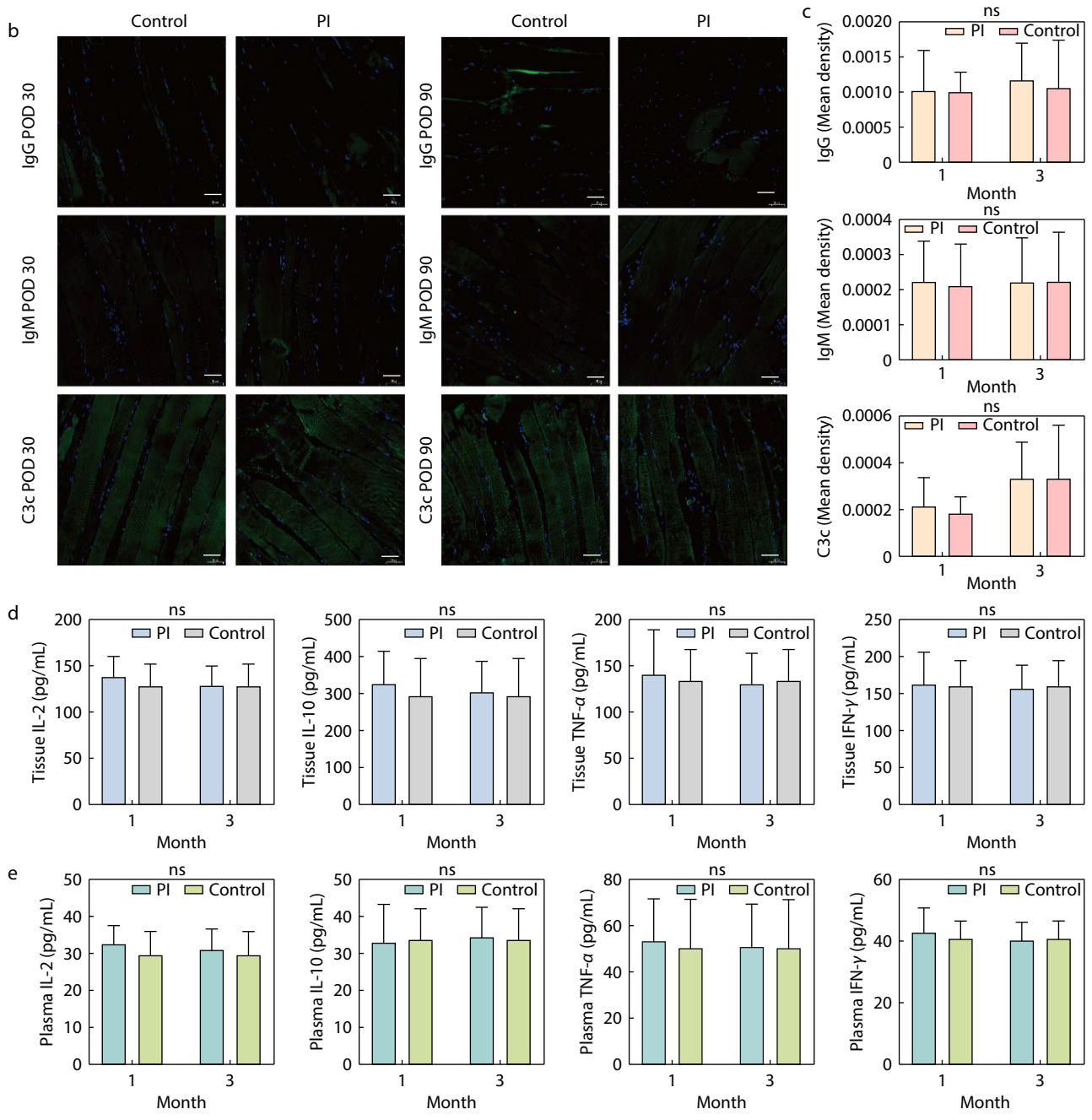

Fig. 5 Evaluation of cuff-related *in vivo* inflammation and immunity. (a) Representative photomicrographs of the hematoxylin and eosin (H&E) staining of the peri-tube muscles of the control and PI groups. Scale bars, 100 μm. (b) Depositions of IgG, IgM, and C3c in peri-tube muscles are shown with immunofluorescence staining. Scale bars, 50 μm. (c) Mean density of peri-tube muscles IgG and, IgM and C3c deposition; (d) Levels of tissue IL-2, IL-10, TNF-*α*, and IFN-*γ* at different time points; (e) Levels of plasma IL-2, IL-10, TNF-*α* and IFN-*γ* at different time points. Data were presented as the mean ± SD (*n*=6 independent samples) (NS: not significant). PI, polyimide; POD, postoperative days.

tion of the cuff tube, and no abnormality was found in the two groups at each time point (Fig. S10b in ESI). Therefore, the H&E staining results and blood biochemical examination illustrated the high biosafety of the PI cuff tube, and there were no functional disorder or organic lesions induced by the tube. Previous studies have reported that PI promising as a safe material for long-term implantation.[25–29] Our findings also confirmed that the PI cuff tube exhibited good *in vivo* biocompatibility and high mechanical strength, and was suitable for use in clinical studies as a long-term implantable devices.

Finally, we systematically compared the operation difficulty, surgical time, vascular injury, patency rate, and target vessel of the hand-sewn suture and several existing mechanical anastomosis devices (Table S10 in ESI). The review results demonstrated that the PI cuff tube is an ideal microvascular anastomotic device for microvessels <1 mm in diameter, which provides a low surgical threshold, reduced anastomo-

sis time, minimized injury, and stable patency rate.[30–40]

CONCLUSIONS

In this study, we successfully fabricated highly stable PI microvascular cuff tubes using the dry-jet wet-spinning method. Through systematic control of the spinning parameters and thermal annealing, the structural and mechanical properties of the tubes were finely tuned to meet the stringent demands of microsurgical vascular anastomosis. The optimized PI cuff tubes demonstrated excellent tensile strength, bending resistance, and compressive recovery, thus outperforming commercial sleeve materials. Extensive *in vitro* and *in vivo* evaluations confirmed their favorable biosafety profiles, including negligible cytotoxicity, genotoxicity, and immunogenicity. Importantly, in a rat hindlimb transplantation model, PI cuff tubes maintained vascular patency and structural stability for at least 90 days post-surgery without inducing local or systemic inflammatory responses. These results validate the PI cuff tube as a robust and biocompatible device for microvascular applications and pave the way for its potential clinical application in microsurgical reconstruction and vascular interventions.

Conflict of Interests

The authors declare no interest conflict.

Electronic Supplementary Information

Electronic supplementary information (ESI) is available free of charge in the online version of this article at http://doi.org/10.1007/s10118-026-3661-2.

Data Availability Statement

The data that support the findings of this study are available from the corresponding author upon reasonable request.

ACKNOWLEDGMENTS

This work was financially supported by the Science and Technology Commission of Shanghai Municipality (No. 22S31904500), the National Natural Science Foundation of China (No. 82102354), and the Fundamental Research Funds for the Central Universities (Nos. 2232025A-02 and CUSF-DH-D-2025006).

REFERENCES

1 Daniel, R.; Olding, M. An absorbable anastomotic device for microvascular surgery. *Plast. Reconstr. Surg.* **1984**, *74*, 337.
2 Moritz, W. R.; Raman, S.; Pessin, S.; Martin, C.; Li, X.; Westman, A.; Sacks, J. M. The history and innovations of blood vessel anastomosis. *Bioengineering (Basel)* **2022**, *9*, 1–17.
3 Robbins, T. H. Microvascular anastomosis: vascular cuff technique. *Plast. Reconstr. Surg.* **1991**, *87*, 1166–1168.
4 Sucher, R.; Lin, C. H.; Zanoun, R.; Atsina, K. K.; Weinstock, M.; Pulikkotil, B.; Schneeberger, S.; Zheng, X. X.; Pratschke, J.; Lee, W. P.; Brandacher, G. Mouse hind limb transplantation: a new composite tissue allotransplantation model using nonsuture supermicrosurgery. *Transplantation* **2010**, *90*, 1374.
5 Hallock, G. G.; Rice, D. C. Use of a microvascular coupler for repair of major distal upper extremity artery injuries. *J. Hand Microsurg.* **2009**, *1*, 3–7.
6 Strunskus, Y.; Grunze, M. Polyimide fundamentals and applications. Marcel Dekker: New York, **1994**, p. 1–350.
7 Klinge, P. M.; Vafa, M. A.; Brinker, T.; Brandis, A.; Walter, G. F.; Stieglitz, T.; Samii, M.; Wewetzer, K. Immunohistochemical characterization of axonal sprouting and reactive tissue changes after long-term implantation of a polyimide sieve electrode to the transected adult rat sciatic nerve. *Biomaterials* **2001**, *22*, 2333–2343.
8 Stieglitz, T.; Beutel, H. R.; Schuettler, M.; Meyer, J. U. Polyimide-based devices for flexible neural interfaces. *Biomed. Microdevices* **2000**, *2*, 283–294.
9 Sun, Y.; Lacour, S. P.; Brooks, R. A.; Rushton, N.; Fawcett, J.; Cameron, R. E. Assessment of the biocompatibility of photosensitive polyimide for implantable medical device use. *J. Biomed. Mater. Res. A* **2009**, *90A*, 648–658.
10 Schmidt, S.; Horch, K.; Normann, R. Biocompatibility of silicon-based electrode arrays implanted in feline cortical tissue. *J. Biomed. Mater. Res.* **1993**, *27*, 1393–1407.
11 Lee, K. K.; He, J.; Singh, A.; Massia, S.; Ehteshami, G.; Kim, B.; Raupp, G. Polyimide-based intracortical neural implant with improved structural stiffness. *J. Micromech. Microeng.* **2004**, *14*, 32–40.
12 Xie, E.; Mei, J.; Xie, S.Y.; Hu, Z.T.; Xi, X.W.; Song, A.Q. ; Yao, B.; Wang, D.Q.; Wei, J.; Niu, Y.F. . Phytic acid-gallium network on a polyimide fiber woven fabric as an artificial ligament for boosting ligament–bone healing and infection treatment. *ACS Appl. Mater. Interfaces* **2024**, *16*, 40726–40738.
13 Zhong, Y.; Wang, Y.; Ma, L.; He, P.; Qin, J.; Gao, J.; Li, J. Ultrasensitive piezoelectric sensor based on polyimide foam for sound recognition and motion monitoring. *ACS Appl. Mater. Interfaces* **2025**, *17*, 11154–11165.
14 Zhao, C.; Park, J.; Root, S. E.; Bao, Z. Skin-inspired soft bioelectronic materials, devices and systems. *Nat. Rev. Bioeng.* **2024**, *2*, 671–695.
15 Zhang, Y.; Jiang, W.; Yuan, S.; Zhao, Q.; Liu, Z.; Yu, W. J. Impacts of a nano-laponite ceramic on surface performance, apatite mineralization, cell response, and osseointegration of a polyimide-based biocomposite. *Int. J. Nanomed.* **2020**, *15*, 9389–9402.
16 Asadullah, S.; Ahmed, M.; Sarfraz, S.; Zahra, M.; Asari, A.; Wahab, N. H. A.; Sobia, F.; Iqbal, D. N. Polyimide biocomposites coated with tantalum pentoxide for stimulation of cell compatibility and enhancement of biointegration for orthopedic implant. *Heliyon* **2023**, *9*, e23284.
17 Tsilimbaris, M. K.; Lit, E. S.; D'Amico, D. J. Retinal microvascular surgery: a feasibility study. *Invest. Ophthalmol. Vis. Sci.* **2004**, *45*, 1963–1968.
18 Santillan, A.; Rubin, D. G.; Foley, C. P.; Sondhi, D.; Crystal, R. G.; Gobin, Y. P.; Ballon, D. J. Cannulation of the internal carotid artery in mice: a novel technique for intra-arterial delivery of therapeutics. *J. Neurosci. Methods* **2014**, *222*, 106–112.
19 Foley, C. P.; Rubin, D. G.; Santillan, A.; Sondhi, D.; Dyke, J. P.; Crystal, R. G.; Gobin, Y. P.; Ballon, D. J. Intra-arterial delivery of AAV vectors to the mouse brain after mannitol mediated blood brain barrier disruption. *J. Control. Release* **2014**, *196*, 71–78.
20 Furtmüller, G. J.; Oh, B.; Grahammer, J.; Lin, C. H.; Sucher, R.; Fryer, M. L.; Raimondi, G.; Lee, W. A.; Brandacher, G. Orthotopic hind limb transplantation in the mouse. *J. Vis. Exp.* **2016**, *110*, e53483.
21 Xu, X.; Kulak, H.; Thür, R.; Caspers, S.; Milis, W.; Tan, X.;

Graphical Abstract

High-performance Polyimide Cuff Tube with Tunable Mechanics and Long-term Biocompatibility for Microvascular Anastomosis

Hui Su, Zhou-Quan Sun, Yu-Cheng Qiu, Yuan-Yuan Zhang, Jing Luo, Fei Liu, Jun Yang, Xian-Yu Zhou, Yue Zhang, and Yu-Mei Zhang

Donghua University; Shanghai Jiao Tong University School of Medicine

P84 polyimide cuff tubes fabricated *via* dry-jet wet-spinning exhibit enhanced mechanical properties after heat treatment and 90-day *in vivo* vascular patency and biosafety.

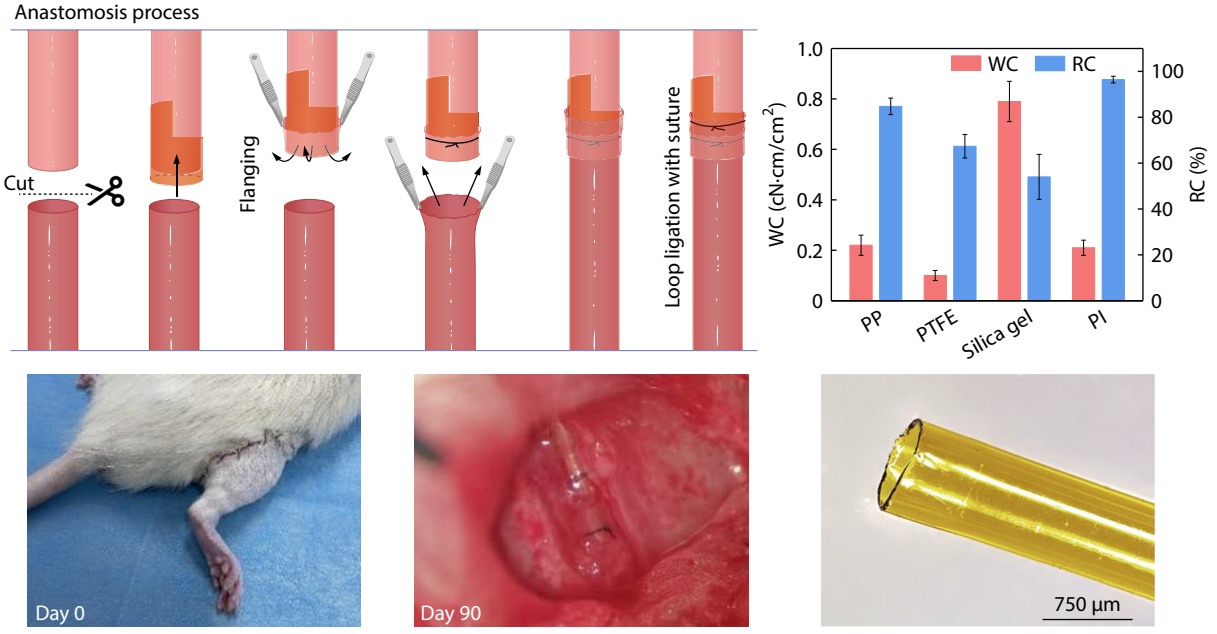

Chinese J. Polym. Sci. 2026, 44, 1898–1911 *https://doi.org/10.1007/s10118-026-3661-2*

Koeckelberghs, G.; Vankelecom, I. F. Thermal treatment effects on separation performance and plasticization resistance of polyimide and PIM-1 membranes. *J. Membr. Sci.* **2025**, *720*, 123792.

22 Sazali, N.; Salleh, W. N. W.; Ismail, A. F.; Ismail, N. H.; Aziz, F.; Yusof, N.; Hasbullah, H. Effect of stabilization temperature during pyrolysis process of P84 co-polyimide-based tubular carbon membrane for H_2/N_2 and He/N_2 separations. *IOP Conf. Ser.: Mater. Sci. Eng.* **2018**, *342*, 012027.

23 Sheng, L.; Ren, J.; Hua, K.; Li, H.; Feng, Y.; Deng, M. The enhancement of mechanical properties of P84 hollow fiber membranes by thermally annealing below and above T_g. *J. Membr. Sci.* **2020**, *595*, 117580.

24 Yu, Y.; Li, J.; Bi, Z.; Wu, C.; Yang, S.; Jiang, Q.; Deng, R.; Fu, Q.; Liu, L.; Wang, C. Cuff anastomosis of both renal artery and vein to minimize thrombosis: a novel method of kidney transplantation in mice. *J. Investig. Surg.* **2022**, *35*, 56–63.

25 Lago, N.; Yoshida, K.; Koch, K. P.; Navarro, X. Assessment of biocompatibility of chronically implanted polyimide and platinum intrafascicular electrodes. *IEEE Trans. Biomed. Eng.* **2007**, *54*, 281–290.

26 Julien, S.; Peters, T.; Ziemssen, F.; Arango-Gonzalez, B.; Beck, S.; Thielecke, H.; Büth, H.; Van Vlierberghe, S.; Sirova, M.; Rossmann, P.; Rihova, B.; Schacht, E.; Dubruel, P.; Zrenner, E.; Schraermeyer, U. Implantation of ultrathin, biofunctionalized polyimide membranes into the subretinal space of rats. *Biomaterials* **2011**, *32*, 3890–3898.

27 Park, G.; Chung, H. J.; Kim, K.; Lim, S. A.; Kim, J.; Kim, Y. S.; Liu, Y.; Yeo, E. H.; Kim, R. H.; Kim, S. S.; Kim, J. S.; Jung, Y. H.; Kim, T. I.; Yee, C.; Rogers, J. A.; Lee, K. M. Immunologic and tissue biocompatibility of flexible/stretchable electronics and optoelectronics. *Adv. Healthc. Mater.* **2014**, *3*, 515–525.

28 Makievskaya, C.; Brezgunova, A.; Andrianova, N.; Kelm, E.; Solovyova, M.; Naumova, G.; Zeinalova, A.; Gancharova, O.; Bushkova, T.; Kozlov, D.; Putlayev, V.; Evdokimov, P.; Petrov, A.; Lebedev, M.; Plotnikov, E.; Popkov, V. Foreign body reaction to neural implants: a comparative study of polymer toxicity and tissue response. *Biosensors* **2025**, *15*, 599.

29 Sirova, M.; Vlierberghe, S. V.; Matyasova, V.; Rossmann, P.; Schacht, E.; Dubruel, P.; Rihova, B. Immunocompatibility evaluation of hydrogel-coated polyimide implants for applications in regenerative medicine. *J. Biomed. Mater. Res. A*

2014, *102*, 1982–1992.
30 Mai, T. T.; Nguyen, L. T. T.; Nguyen, P. D. Efficiency and safety of microvascular anastomotic coupler for wrist revascularization in traumatic injuries. *JPRAS Open* **2024**, *41*, 252–259.
31 Arora, R.; Mishra, K. S.; Bhoye, H. T.; Dewan, A. K.; Singh, R. K.; Naalla, R. Mechanical anastomotic coupling device versus hand-sewn venous anastomosis in head and neck reconstruction-an analysis of 1694 venous anastomoses. *Indian J. Plast. Surg.* **2021**, *54*, 118–123.
32 Ilie, V.; Haddad, R.; Moisidis, E. Sutureless microvascular anastomosis: literature review. *Int. Microsurg. J.* **2019**, *3*, 1–9.
33 Park, U. J.; Jeong, W.; Kwon, S. Y.; Kim, Y.; Choi, K.; Kim, H. T.; Son, D. Fabrication of a novel absorbable vascular anastomosis device and testing in a pig liver transplantation model. *Ann. Biomed. Eng.* **2019**, *47*, 1063–1077.
34 Jeong, W.; Kim, K.; Son, D.; Kim, Y. New absorbable microvascular anastomotic devices representing a modified sleeve technique: evaluation of two types of source material and design. *Sci. Rep.* **2019**, *9*, 10945.
35 Ribaudo, J. G.; He, K.; Madira, S.; Young, E. R.; Martin, C.; Lu, T.; Sacks, J. M.; Li, X. Sutureless vascular anastomotic approaches and their potential impacts. *Bioact. Mater.* **2024**, *38*, 73–94.
36 Hoogewerf, M.; Schuurkamp, J.; Kelder, J. C.; Jacobs, S.; Doevendans, P. A. Sutureless versus hand-sewn coronary anastomoses: a systematic review and meta-analysis. *J. Clin. Med.* **2022**, *11*, 749.
37 Klima, U.; Falk, V.; Maringka, M.; Bargenda, S.; Badack, S.; Moritz, A.; Mohr, F.; Haverich, A.; Wimmer-Greinecker, G. Magnetic vascular coupling for distal anastomosis in coronary artery bypass grafting: a multicenter trial. *J. Thorac. Cardiovasc. Surg.* **2003**, *126*, 1568–1574.
38 Vicol, C.; Eifert, S.; Oberhoffer, M.; Boekstegers, P.; Reichart, B. Mid-term patency after magnetic coupling for distal bypass anastomosis in coronary surgery. *Ann. Thorac. Surg.* **2006**, *82*, 1452–1456.
39 Lu, Q.; Liu, K.; Zhang, W.; Li, T.; Shi, A. H.; Ding, H. F.; Yan, X. P.; Zhang, X. F.; Wu, R. Q.; Lv, Y.; Wang, S. P. End-to-end vascular anastomosis using a novel magnetic compression device in rabbits: a preliminary study. *Sci. Rep.* **2020**, *10*, 5981.
40 Yang, L.; Lu, J.; Wang, Y.; Zhang, M.; Shi, Y.; Wei, S.; Liu, P.; Wu, Z.; Lv, Y.; Wu, R. A rat model of orthotopic liver transplantation using a novel magnetic anastomosis technique for suprahepatic vena cava reconstruction. *J. Vis. Exp.* **2018**, *133*, 56933.

https://doi.org/10.1007/s10118-026-3661-2